DEDUCING NON-MIGRATING DIURNAL TIDES IN THE EARTH'S THERMOSPHERE USING SATELLITE DATA FROM THE NASA GLOBAL-SCALE OBSERVATIONS OF THE LIMB AND DISK (GOLD) MISSION

Christopher S. Krier
Faculty Advisor: Scott England
Kevin T. Crofton Department of Aerospace and Ocean Engineering, Virginia Tech

Abstract

One pathway to troposphere-thermosphere coupling is the upward propagation of non-migrating tides (planetary-scale atmospheric waves whose generation mechanisms include solar absorption by the atmosphere, large-scale tropical convection, and wave-wave interaction). At present, there is a gap of observational constraints on these tides in middle thermosphere temperature, and their impact on thermospheric composition is not well understood. In geostationary orbit, above the mouth of the Amazon River, the Global-scale Observations of the Limb and Disk (GOLD) mission flies a two-channel far ultraviolet spectrometer that provides valuable daytime images of neutral temperature and the column density ratio of atomic oxygen to molecular nitrogen (O/N_2). Here, we summarize advances made in accomplishing our objective to deduce the dominant non-migrating diurnal tides from the combined temperature-O/N_2 dataset from GOLD. We present results and their associated uncertainties from application to GOLD data for two different seasons. A lesson we have learned is that solar zenith angle effects and ionospheric contamination are important considerations when deriving tides using far ultraviolet column emissions. We show that our approach is a powerful tool for probing the variability of non-migrating tides in a region of near-Earth space where they are poorly characterized.

1. Introduction

Human civilization has become increasingly more dependent on space-based technologies such as radio communication, global navigation satellite systems (GNSS), and remote sensing. It is therefore tremendously important to achieve operational forecasting of space weather and climate. It has only been recently discovered that the near-Earth space environment is strongly coupled to the lower atmosphere through upward propagating atmospheric waves. Solar atmospheric tides are persistent large-scale waves in the neutral atmosphere that are principally forced by absorption of solar radiation. Solar atmospheric tides have components which have periods that are subharmonics of a solar day and zonal wavelengths that are integer fractions of circles of latitude. Non-migrating diurnal tides are the non-Sun-synchronous components of atmospheric tides that have periods equal to a solar day. Many of these components propagate into the thermosphere from forcing regions in the troposphere. *Leonard et al.*, [2012] showed that non-migrating tides in neutral density need to be considered to accurately predict the orbital and reentry drag environments. Perturbations caused by a tide with period n and zonal wavenumber s varies in universal time t and longitude λ according to the following formula:

$$A_{n,s}\cos\left(n\Omega t + s\lambda - \phi_{n,s}\right) \quad (1)$$

Where, where $s < 0$ denotes eastward propagation, Ω is the rotation rate of the Earth, $A_{n,s}$ is the tidal amplitude, and ϕ is the tidal phase (typically defined as the universal time of maximum at 0 degrees longitude). Tidal amplitudes and phases are functions of latitude and altitude. It is useful to analyze measurements from spacecraft in the local time frame. A simple conversion between local time t_{LT} and universal time is the following:

$$t_{LT} = t + \lambda/\Omega. \quad (2)$$

Substituting Eqn. 2 into Eqn. 1 yields:

$$A_{n,s}\cos\left(n\Omega t_{LT} + (s-n)\lambda - \phi_{n,s}\right) \quad (3)$$

Migrating tides, $n = s$, are thus longitudinally invariant while non-migrating tides, $n \neq s$, control longitudinal variability at a fixed local time. Evidently, viewing a tidal component in the local time frame doppler shifts its zonal wavenumber as a result of viewing the tidal component in a reference frame that is rotating westward relative to the universal time frame. The naming convention of tidal components used in this paper is as follows. The name of a tidal component begins with its period: (D = diurnal, S = semidiurnal, T = terdiurnal), followed by its horizontal propagation direction: (E = eastward, W = westward, no letter included in the case of stationary wave), and ends with its zonal wavenumber in the universal time frame. For example, DE3 propagates eastward with diurnal period and zonal wavenumber-3 and S0 is the stationary semidiurnal component.

Global-scale Observations of the Limb and Disk (GOLD) is a NASA mission of opportunity which began science operations in October 2018. GOLD is an exciting pathfinder in the NASA Heliophysics fleet of missions currently in orbit. This research project uses GOLD daytime images of middle thermosphere temperature and composition. The thermosphere is the uppermost region of Earth's atmosphere and is characterized by its sharp temperature gradients, diffusively separated neutral constituents, as well as its coupling to the ionosphere. One of the scientific objectives of GOLD is to quantify the impact of atmospheric tides on the temperature structure of the thermosphere [*Eastes et al.*, 2017]. There is an observational gap of non-migrating tides in middle thermosphere temperature, and the impact of these tides on middle thermospheric composition has not been well characterized. The purpose of this research project is to deduce non-migrating diurnal tides from the combined temperature-composition dataset from GOLD.

This research paper is organized as follows. Section 2 describes the data used herein, Section 3 provides an overview of our approach to deducing non-migrating diurnal tides, Section 4 presents an application to GOLD observations from two different seasons, and Section 5 summarizes presentations given by the author related to this research.

2. Data

2.1 GOLD Dataset

The GOLD mission employs two far-ultraviolet imaging spectrographs onboard the SES-14 telecommunications satellite in geostationary orbit at 47.5° West [Eastes et al., 2017]. The two identical and independent channels (A and B) of the GOLD instrument measure emissions from 132 to 162 nm of the limb and disk in its field-of-regard which encompasses much of North and South America, the Atlantic Ocean, and West Africa (Figure 1).

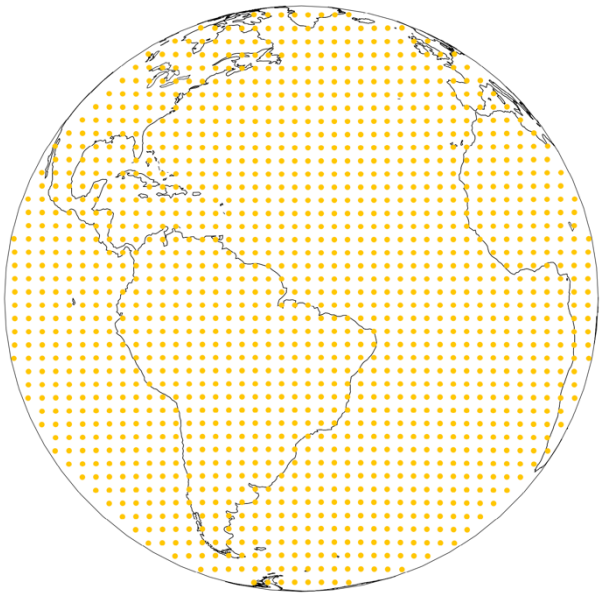

Figure 1. GOLD field-of-regard. The pixel centers of the daytime images of disk neutral temperature and O/N_2 column density ratio are shown as filled-in gold circles.

GOLD performs dayside disk scans ~68 times each day at 30-minute cadence. The northern and southern hemispheres are scanned separately. GOLD infers disk neutral temperature from the rotational structure of N_2 LBH band system emissions, ~2/3 of which comes from within one scale height of the altitude of peak emission. The retrieved disk neutral temperature is thus an effective, column integrated quantity that is weighted heavily by the peak of the N_2 LBH volume emission rate (photons cm^{-3} s^{-1}). Since the peak altitude of emission increases with solar zenith angle (SZA), there is a weak (<20%) dependence of the GOLD effective temperature on SZA, particularly above ~60°. GOLD infers the column number density ratio of atomic oxygen to molecular nitrogen (O/N_2) from the ratio of atomic oxygen 135.6 nm and molecular nitrogen LBH band emission intensities. GOLD only retrieves disk neutral temperature and O/N_2 ratio for SZA < 80° and EMA < 75°.

2.2 TIE-GCM Simulations

Our approach (discussed in Section 3) leverages temperature-composition tidal phase differences obtained from the NCAR Thermosphere-Ionosphere-Electrodynamics General Circulation Model (TIE-GCM) [Richmond et al., 1992]. TIE-GCM is a nonlinear and three-dimensional representation of the coupled thermosphere-ionosphere system. As a model of the GOLD disk neutral temperature, we calculate effective neutral temperature by weighting neutral temperature profiles by a contribution function. The contribution function, essentially a normalized emission rate profile of the LBH band, depends on solar zenith angle and emission angle (the angle between the look direction and nadir). Shown in Figure 2 is the modeled contribution function for several solar zenith angles (whose colors are indicated by the legend) in the case of nadir viewing. Also shown in Figure 2, indicated by the red line, is a typical neutral temperature profile in the middle thermosphere. It can be seen that the peak of the contribution function increases in altitude and broadens for higher solar zenith angles. Comparing this to the neutral temperature profile, there is a clear dependence on the effective neutral temperature on SZA. For the purpose of computing *a priori* tidal phase differences using TIE-GCM output, we apply a uniform contribution function (SZA = 78° and EMA = 0°) to all data points. This is justified because the contribution function does not depend on EMA for high SZA and, as discussed in Section 3, our approach uses only dawn and dusk data. It was found that when SZA is allowed to vary, the tides in effective temperature are significantly distorted as a result of SZA effects which

vary with local time, latitude, and season (not shown).

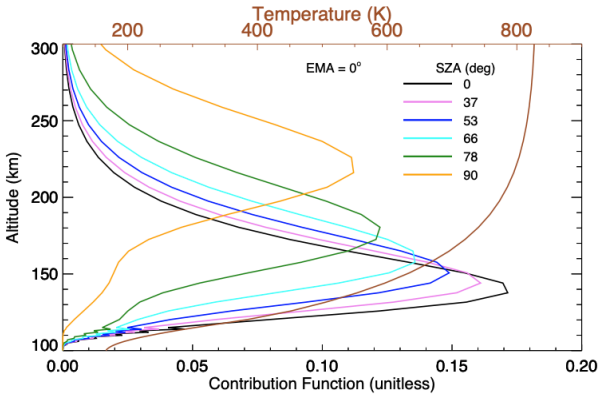

Figure 2. Modeled contribution function for several solar zenith angles (see legend) in the case of nadir viewing. Shown in red is a typical neutral temperature profile.

As a model of the O/N_2 ratio, we compute the vertical O column densities relative to a reference N_2 depth of 10^{17} cm^{-2} [Strickland et al., 1995]. Tidal decomposition of the modeled neutral temperature and O/N_2 ratio is performed via two-dimensional FFTs. Figure 3 shows the latitudinal amplitude structure of temperature and O/N_2 ratio for the most important non-migrating diurnal tides in January and solar minimum conditions. DE3 and DE2 are the dominant tides during this season. In October, DE3 is the most dominant non-migrating diurnal tide (not shown).

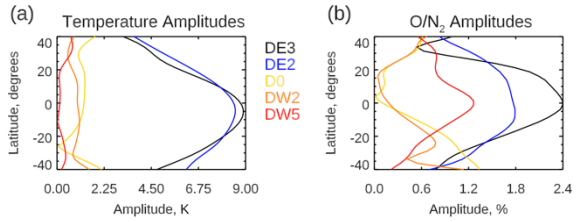

Figure 3. Temperature (Kelvins) and O/N_2 (percent relative to zonal mean) amplitudes versus latitude for select non-migrating diurnal tides in January and solar minimum conditions.

3. Methodology

Traditional Fourier methods cannot be applied to the GOLD dataset because there is incomplete coverage in longitude and local time. Therefore, a novel approach is needed. We have developed an approach that deduces two specified non-migrating diurnal components. The approach is limited to deducing only two components as a result of the limited spatial-temporal sampling and computational expense. Our algorithm is discussed in detail in last year's report. What makes our approach unique is the simultaneous retrieval of tides in both temperature and composition (O/N_2). Our approach enforces consistency between the deduced tides by leveraging modeled temperature-O/N_2 tidal phase differences obtained from the NCAR Thermosphere-Ionosphere-Electrodynamics General Circulation Model. A short description of our approach is provided here. First, we form dusk – dawn differences at each spatial pixel thereby removing odd harmonics within local time variations and leaving diurnal variations (assuming higher order even harmonics are negligible) since these local times are close to 12 hours apart. Residuals from the zonal mean of these diurnal variations are converted to dimensionless units and normalized and serve as the data used to determine the tidal parameters. We determine the most probable tidal parameters by performing a least squares fit on temperature and O/N_2 at the same time while constraining the tidal phases. In order to shorten runtime, we have implemented a pattern search optimization routine, a type of direct search method. When working with the GOLD data it became apparent that a number of additional data treatment steps needed to be done in order to make extraction of the non-migrating diurnal tides easier. This included taking averages over time periods, removal of linear trends with longitude, smoothing, and interpolation to an evenly spaced longitude grid. Also, our approach was

modified to allow some deviation (+/- 10° longitude of phase) from the modeled phase difference.

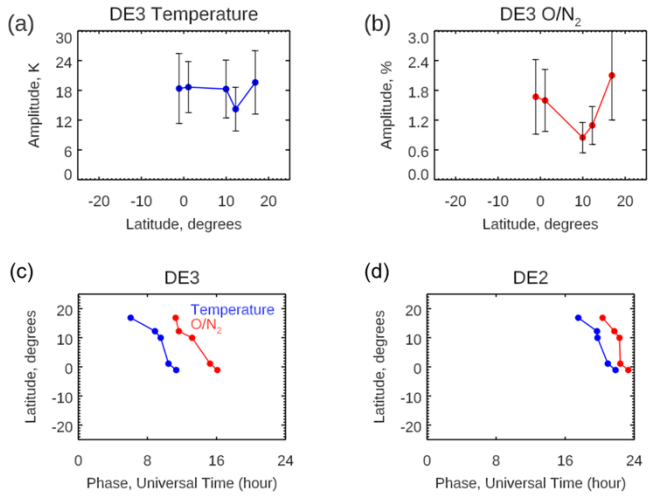

Figure 4. Retrieved tidal parameters versus latitude during time period in October 2018. (a) and (b) show DE3 amplitude in temperature (Kelvins) and O/N_2 (percent relative to zonal mean) respectively. Error bars represent the root mean square deviation of the least squares fit and provides a measure of uncertainty. (c) and (d) show DE3 and DE2 phase in temperature (blue) and O/N_2 (red).

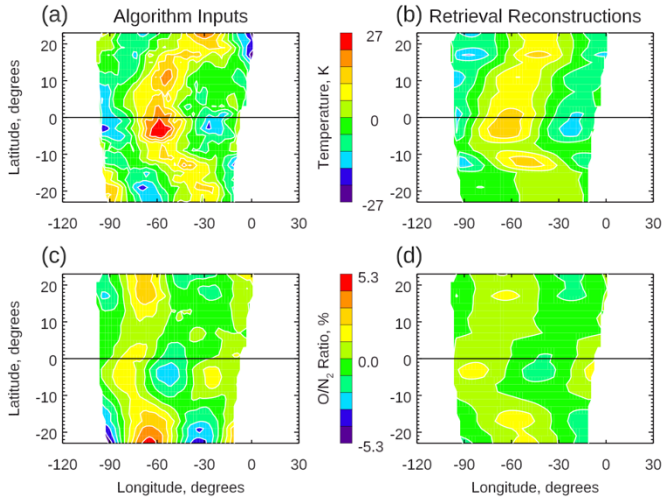

Figure 5. Global maps of the dusk-dawn differences and retrieved tides for temperature, (a) and (b), and O/N_2, (c) and (d), for the time period in October 2018.

4. Application to GOLD Data

We analyze GOLD data taken from two time periods during different seasons: 14-27 October 2018 and 1-31 January 2020. These fitting periods are selected as times when non-migrating tides are strong and somewhat different and to avoid times when rapid changes occur. Our analysis is conducted between -25°

and 25° latitude where the non-migrating tides of interest are strongest.

4.1 October 2018

During northern hemisphere autumn, DE3 is expected to be the dominant non-migrating diurnal tide. Figure 4 shows the retrieved DE3 tidal parameters in addition to DE2 phases. These plots only show retrievals at latitudes where the retrieved DE3 amplitude (for both temperature and O/N_2) is at least two times greater than the root mean square deviation (RMSD) of the least squares fit. These retrievals correspond to those with the lowest uncertainty in the retrieved DE3 tidal parameters. The error bars in figures 4a and 4b indicate the RMSDs. In temperature, the DE3 amplitude is nearly constant with latitude ~ 18 Kelvins. This provides an estimate of DE3 temperature amplitude in an altitude region where it has never before been observed. It is noteworthy that it is appreciably larger than that modeled by TIE-GCM (~7 K). In O/N_2, there is a dip in the retrieved DE3 amplitude around 10° N. (c) and (d) show DE3 and DE2 phases slope to early universal times going from south to north. Figure 5 shows a comparison of the dusk-dawn differences and the retrieved tides in the form of global maps (latitude vs. longitude). These show the retrieved tides at all latitudes (even at latitudes that surpass our uncertainty threshold). It is seen that our approach reproduces the dusk-dawn differences only when the GOLD temperature and O/N_2 are slightly out of phase as predicted by TIE-GCM. When temperature and O/N_2 perturbations are 90° longitude out of phase, as is the case around 20° S, our approach is not able to reproduce the dusk-dawn differences because the constraint on the tidal phase does not allow it. The lack of latitudinal symmetry in the GOLD data, a departure from TIE-GCM, suggests that (1) tidal dissipation is probably different in the model than the real atmosphere observed by GOLD, (2) more than two tides are present, and/or (3) instrument or algorithm artifacts alias into the tides.

4.2 January 2020

During northern hemisphere winter, DE3 and DE2 are expected to be the dominant non-migrating diurnal tides. Figure 6 shows the retrieved DE3 and DE2 tidal parameters. Analogous to the above, these plots only show retrievals at latitudes where the retrieved DE3 amplitude (for both temperature and O/N_2) are at least two times greater than the root mean square deviation (RMSD) of the least squares fit. In temperature, the DE3 and DE2 amplitudes, (a) and (c) are higher south of the equator than north of the equator. In O/N_2, there are dips in the DE3 and DE2 amplitudes around 3° N. The retrieved DE3 and DE2 phases are approximately constant with latitude. It is noteworthy that the retrieved DE3 temperature and O/N_2 phases are approximately the same phase. This is unexpected for an eastward propagating wave, whose temperature phase is expected to be earlier in UT as is the case for Figures 4c, 4d, 6f, and the modeled DE3 and DE2 phases (not shown). The result in Figure 6e happens because our approach allows some variation in the phase difference constraints (Section 3). This inconsistency is likely the result of a combination of the factors discussed above in Subsection 4.1. Figure 7 is the same as Figure 5 but for the time period in January 2020. As is the case for the time period in October 2018, there are latitudes where the temperature-composition phase offset in the GOLD observations do not match those in TIE-GCM.

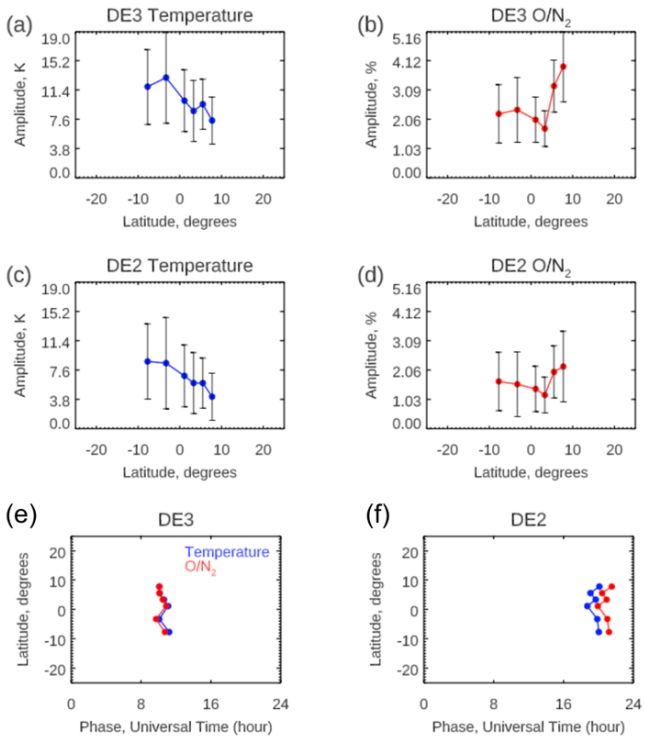

Figure 6. Analogous to Figure 4 but for January 2020 and now the DE2 amplitudes are included.

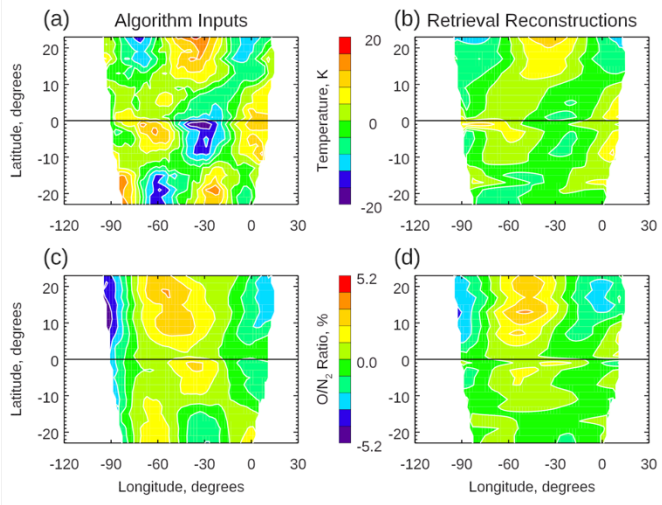

Figure 7. Same as Figure 5 but for January 2020.

4.3 Does ionospheric contamination impact the deduced tides?

Previous studies (Kil et al., [2013] and references therein) have shown that thermospheric O/N_2 ratio retrieved from far-ultraviolet dayglow are contaminated by O^+ radiative recombination in the ionosphere, concentrated around the equatorial ionization anomaly (EIA), which emits at the same wavelength, 135.6 nm, used in the O/N_2 retrieval. Kil et al. [2013] concluded that the longitudinal wave patterns in GUVI O/N_2 near 15:00 LT mostly reflect the ionosphere 135.6 nm emissions. The tidal variations in the O^+ radiative recombination likely correlate with those in F-region plasma density which are driven by E-region dynamo modulation by tidal winds. In general, the O/N_2 tidal signatures near the EIA may be produced by a superposition of the thermospheric tides and the ionospheric contamination, which should both have the same wavenumber structure but may be out of phase. It is expected that O/N_2 near the morning terminator is less impacted by the ionosphere (since nighttime recombination depresses the O+ density). In the following, we assess the potential impact of ionospheric contamination on the O/N_2 non-migrating diurnal proxies used in our approach. GOLD has the unique advantage of measuring post-sunset 135.6 nm emissions of the ionosphere in the same sector of the Earth over which O/N_2 is retrieved during daytime. We use GOLD night scans to construct a map of post-sunset 135.6 nm emissions by averaging into a local time bin extending from 19:00-22:00 LT. These maps serve as a proxy for the ionospheric contribution to 135.6 nm emissions around dusk used in the O/N_2 retrieval. The maps analyzed reflect the average of the respective time periods in October 2018 and January 2020. Note that when analyzed in the same fashion, the dusk/dawn difference of the ratio of the 135.6 nm and LBH band (135.6/LBH) intensities correlate extremely well (not shown) with those of O/N_2 (since O/N_2 is derived from 135.6/LBH; plotted in Figures 5 and 7). We can therefore assess the potential impact of ionospheric contamination on our approach by first removing the post-sunset 135.6 nm emissions from the dusk 135.6 nm emissions used in the retrieval of O/N_2 and then recomputing the 135.6/LBH ratio. Figures 8a and 8b compare 135.6/LBH brightness ratios before and after the post-sunset 135.6 nm emissions are removed for the period during October 2018. Note the loss of longitudinal coverage is because GOLD does not perform night scans in the entire region over which GOLD performs day scans. Figure 8c maps the difference of the 135.6/LBH before and after treating for ionospheric contamination. This difference resembles the map of post-sunset 135.6 (Figure 8d) used in the removal. The geomagnetic equator is indicated in Figure 8d as a dashed line and the brightest post-sunset 135.6 nm emissions clearly follow the equatorial arcs and also exhibit longitudinal asymmetry, especially in the southern hemisphere. By looking at Figure 8d and by comparing Figures 8a and 8b, we can conclude that while the ionospheric contamination does not seem to impact the phase of the 1356/LBH pattern in October 2018, it does appreciably affect the amplitude and longitude asymmetry, but not enough to fully explain the morphology responsible for the discrepancy with TIE-GCM simulation. This analysis was also done for the time period in January 2020 and the impact of the ionosphere is negligible (not shown).

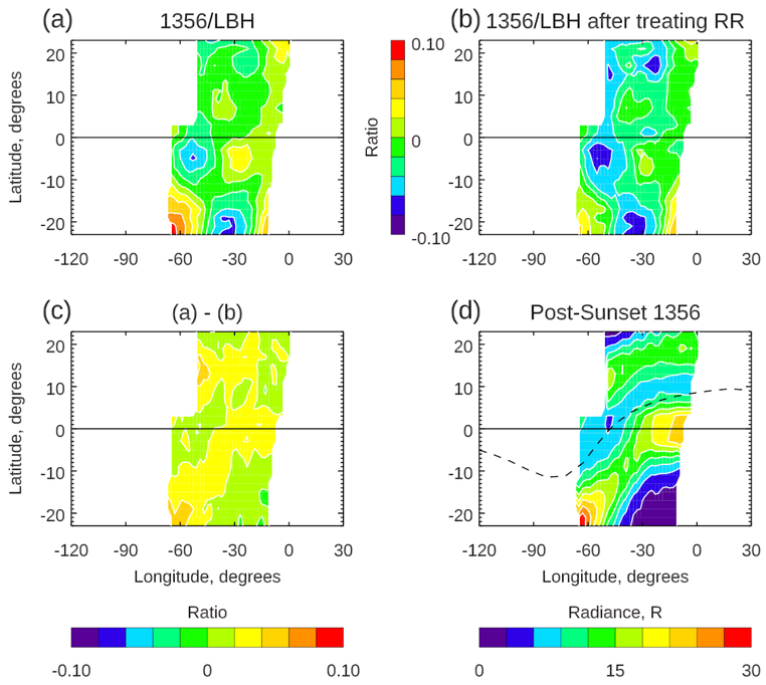

Figure 8. Dusk-dawn differences of 1356/LBH ratios before (a) and after (b) O+ RR is treated. (c) shows the difference of (a) and (b). The global map (d) of post-sunset 1356 used in the O+ RR treatment. The dashed line indicates the geomagnetic equator.

Ionospheric contamination has a seasonal dependence such that our results in October 2018 are more likely to be impacted by ionospheric contamination. It is conceivable to produce a revised GOLD O/N_2 product where the post-sunset 135.6 nm emissions are removed from the retrieval input near dusk, but this is beyond the scope of the current work. From the above analysis, we surmise that the ionospheric signature in GOLD O/N_2 non-migrating tides is minimal due to the pronounced dip in the magnetic equator with respect to the geographic equator across the Earth in GOLD's field-of-regard. This geometry tends to smooth out any ionospheric signature in the non-migrating tides.

5. Summary of Presentations

The author presented a virtual poster at the 2020 AGU Fall Meeting in a session titled “Drivers and Prediction of Variability in Earth’s Ionosphere and Thermosphere: New Observations from Missions”. A manuscript based on some of the research discussed in this report is currently in preparation for submission to the *Journal of Geophysical Research: Space Physics*. The author presented a research update at the September 2020 GOLD Science Team Meeting and will again do so at the same meeting taking place virtually April 12-14 2021.

Acknowledgements

The author would like to express his gratitude to the Virginia Space Grant Consortium for providing additional financial and travel support during the past two academic years. The author would like to acknowledge J. S. Evans and J. Correira (both from Computational Physics, Inc.) for providing reprocessed GOLD TDISK and ON2 files. We also acknowledge K. Greer (University of Colorado Boulder) for providing TIE-GCM model output used in this analysis. GOLD Level 2 data are available from the GOLD Science Data Center (http://gold.cs.ucf.edu/search/) and the NASA Space Physics Data Facility (https://spdf.gsfc.nasa.gov).

References

Eastes, R. W., McClintock, W. E., Burns, A. G., Anderson, D. N., Andersson, L., Codrescu, M., et al. (2017). The Global-scale Observations of the Limb and Disk (GOLD) mission. *Space Science Reviews*, 212(1-2), 383–408. https://doi.org/10.1007/s11214-017-0392-2.

Evans, J. S., D. J. Strickland and R. E. Huffman (1995), Satellite remote sensing of thermospheric O/N_2 and solar EUV: 2. Data analysis, *J. Geophys. Res.*, Vol. 100, NO.A7, pages 12,227-12,233.

Kil, H., W. K. Lee, J. Shim, L. J. Paxton, and Y. Zhang (2013), The effect of the 135.6 nm emission originating from the ionosphere on the TIMED/GUVI O/N_2 ratio, *J. Geophys. Res. Space Physics*, 118, 859–865, doi:10.1029/2012JA018112.

Leonard, J. M., J. M. Forbes, and G. H. Born (2012), Impact of tidal density variability on orbital and reentry predictions, *Space Weather*, 10, S12003, doi:10.1029/2012SW000842.

Richmond, A. D., E. C. Ridley, and R. G. Roble (1992), A thermosphere/ionosphere general circulation model with coupled electrodynamics, *Geophys. Res. Lett.*, 6, 601-604.